Available online at www.sciencedirect.com

jmr&t Journal of Materials Research and Technology

journal homepage: www.elsevier.com/locate/jmrt

Original Article

Effects of tool–workpiece interfaces friction coefficient on power and energy consumption during the piercing phase of seamless tube production

Hamed Aghajani Derazkola[*], *Eduardo Garcia*, *Alberto Murillo-Marrodán*

Department of Mechanics, Design and Industrial Management, University of Deusto, 48007 Bilbao, Spain

ARTICLE INFO

Article history:
Received 30 March 2022
Accepted 12 June 2022
Available online 17 June 2022

Keywords:
Hot piercing process
Seamless tube
Energy consumption
Super Cr13 steel

ABSTRACT

This research analyzes the impact of various friction conditions at the interface of the tube piercing machine tools and Super Cr13 steel workpiece. For this reason, the three-dimensional finite element method (FEM) is employed in the simulation of the tube piercing process. The friction conditions are simulated considering Tresca, Viscoplastic, IFUM and Neumaier models which have been implemented at the Rollers-Billet (RF), Plug–Billet (PF), and Diescher–Billet (DF) interfaces. After testing their performance, Visco-plastic is selected for RF interface, and Tresca for PF and DF interfaces, respectively. Additionally, a friction coefficient range between 0.01 and 0.6 is used for RF, 0.06–0.15 for PF, and 0.1–0.3 for DF. The relation between normal stress, strain, temperature, and quality of pierced tubes is discussed, as well as the connection between the friction coefficient and the energy consumption. The FEM results are validated by actual piercing process data provided by Industry. The results show that the normal stress on billet during piercing increases by increasing friction on RF interface. With increasing friction in PF, both friction power and plastic power increase, while increasing friction in RF lead to a friction and plastic power decrease. According to the results, the minimum energy consumption is recorded at RF = 0.5, PF = 0.06, and DF = 0.1.

1. Introduction

The early-stage during seamless tube manufacturing is the tube piercing phase (TPP). In this phase, a pre-cut billet with specific dimensions and geometry is heated up to more than 80% of its melting temperature, until it is converted to plasticized form [1]. After that, the tooling system which consists of a roller and side guiding tool (rotational Diescher disks or static guiding shoes) push the heated billet forward and, at the same time, a hard tool called plug starts to pierce the billet [2]. In this step, the hot billet is pierced inside, elongated and its thickness reduced [3]. Usually before

* Corresponding author.
E-mail address: h.aghajani@deusto.es (H. Aghajani Derazkola).
https://doi.org/10.1016/j.jmrt.2022.06.071

piercing, the a cavity in the center of the billet is created by ductile damage, a phenomenom known as the Mannesmann effect [4]. During TPP, rollers rotate with axes offset that is called feed angle. The number of rollers in TPP could be at least two or more. The main role of the rollers is pushing forward the hot billet against the plug direction. On the other hand, the side tool guides the billet and controls the produced tube's dimension [5]. The forward movement generated by rollers continues until the full billet is pierced into a hollow tube. Tool shapes, feeding angle, and normal axis pressure are critical parameters for precise dimensions, defect-free, and good surface quality [6].

Among all parameters in this process, Friction, as a physical phenomenon at the interface of tools and workpiece, plays a prominent role. The Friction at high temperature determines material flow, producibility and energy consumption during this process. From a geometrical point of view, the Friction occurs between rollers-workpiece, plug-workpiece, and guiding tool–workpiece interfaces [7]. From a manufacturing point of view, the frictional contact between

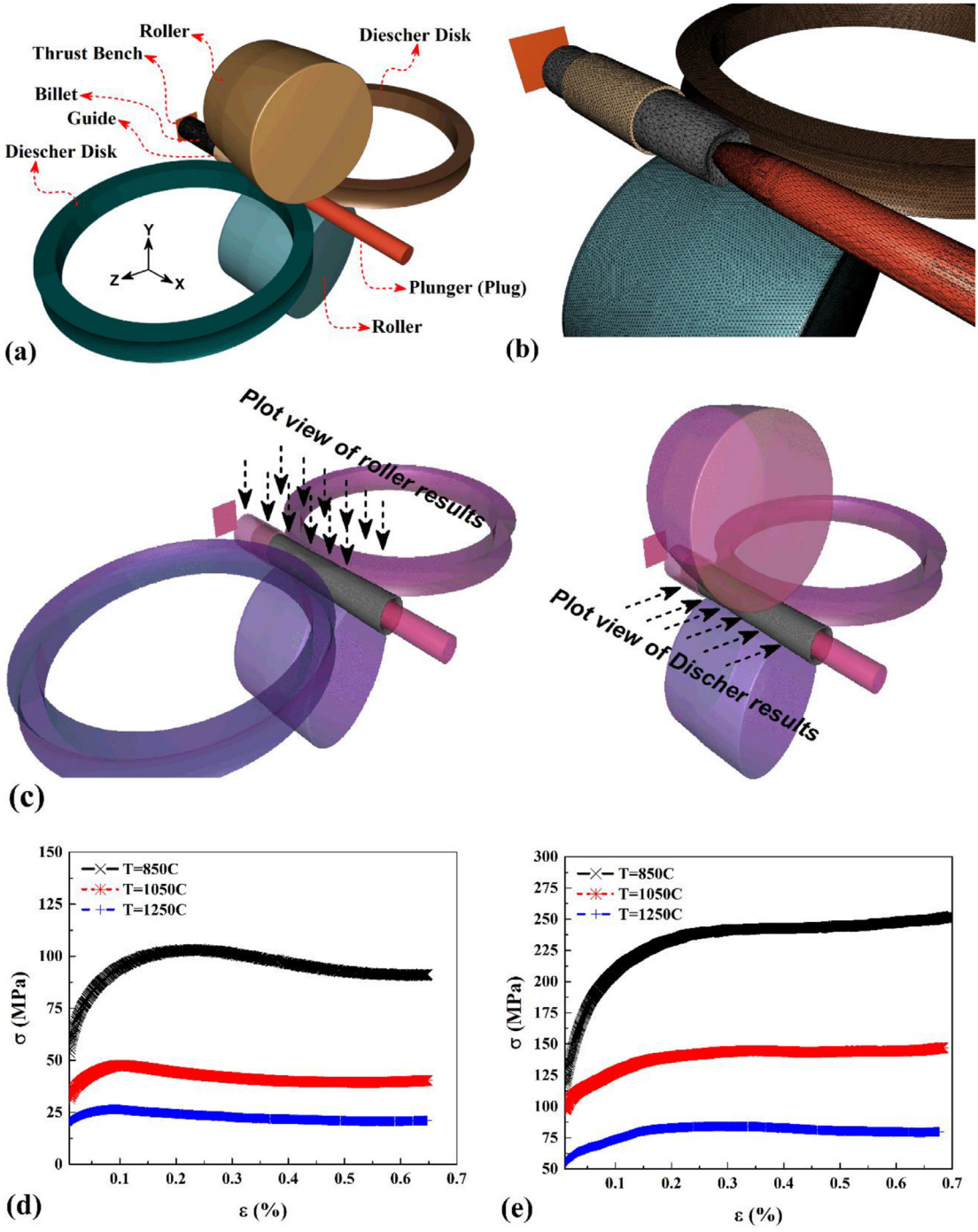

Fig. 1 – (a) Schematic view of simulation domain, (b) meshed model, (c) constitutive model chosen for Cr13 super steel various temperature and 10s^{-1} strain rate.

rollers and workpieces is much higher than in other tools–billet interfaces. The high friction at rollers-billet contact area is responsible for the rotational and forward movement of the tube generating the inner crack (Mannesmann effect) in front of the plug and finally piercing the tube. During the piercing process, the plug freely rotates on its axis, and the friction resistance in the piercing direction is essential [8].

During TPP, the Diescher disks have angular velocity and friction at the Diescher–Billet interface is not high. For this reason, the prominent role of Diescher disks in TPP is controlling the geometry of pierced tube and helping the forward drive of the billet [9]. The friction in this area does not significantly affect materials flow compared to other tools. For the production of a sound tube, the driving friction on both the roller-workpiece and guides-workpiece should be balanced with plug friction condition. Owning to the complication of the TPP stage during the seamless tube production process, limited three-dimensional FEM studies have been published to understand thermo-mechanical phenomena between tooling system and workpiece [10]. The tooling forces, temperature, and friction are critical physical factors that affect final product geometry and metallurgical quality [11]. The available literature studied the TPP with two main scopes. First, physical-chemical phenomena during TPP involved in the Mannesmann effects (crack opening), final metallurgical properties, temperature changes, and ductile damage model. Second, manufacturing and tooling systems consist of positioning plug and rollers, plug and roller shapes, and contact conditions between tools and workpiece [12].

The friction, which affects the metallurgical surface quality, crack type, and piercing features during TPP, can be affected by workpiece materials and process parameters. Recently, Murillo-Marrodán et al. [13] addressed various friction models at the interface of plug and rollers during the TPP phase of 9Cr steel. The FEM software is used to understand thermo-physical phenomena during the TPP phase like cross-roll force and torque to analyze power consumption, TPP process efficiency, and analysis of tube twisting. Fernandes et al. [10] simulated the TPP phase to investigate the effects of friction non-uniformity on cross-rolls, piercing plug, and Diescher disks. They validated their results with experimental data on S355 steel and concluded that the plug friction could be determined based on plug force. Also, the friction of Diescher directly related to the force and torque of the Diescher disk. According to available literature, the effects of friction condition between the tooling system and super chromium steel on strain rate and total consumption energy at the TPP phase have not been considered [14]. The main focus of previous research was on the process parameters. On the other hand, one of the central issues in this process is the relation between physical phenomena and another technical area. Energy consumption is one of the critical aspects of the manufacturing process that affects the ecosystem for decreasing environmental pollution and is valuable to industries to decrease the final product price. This article aims to study various friction conditions between the tooling system and super Cr13 steel to minimize energy consumption during the TPP phase, which has not been considered before.

2. Process modeling

2.1. Geometries and process domain

The simulation domain in this study consists of super Cr13 steel billet, pusher, Guide, rollers, Diescher disks, and Plug geometries. The geometry and positioning of tools and billet were selected according to the experimental procedure. The billet had 202 mm diameter and 600 mm length. The rollers had a 900 mm diameter with a 1.5° profile angle, 0° cross angle, and 12° feed angle. During the simulation process, the rollers had a 111 rpm rotational speed. In the simulation domain, a guide with a 208 mm diameter was selected to position billet during forward-moving at the early stage of the process and a thrust bench for pushing billet. In this study, the thrust bench velocity 100 mm/s was selected. A Plug with free rotation velocity and two Diescher disks were designed at both sides of the billet to improve the geometrical accuracy of the final product. Fig. 1a depicts the simulation domain.

2.2. Finite element model

The simulation domain of the skew rolling milling stage drawn by CAD software was imported into FORGE® NxT (Version 3.2) and meshed (Fig. 1b) to solve the problem. The rotational and traverse velocities were set according to the experimental tests mentioned above. For simplicity of the simulation, all tools were selected as non-deformable (rigid) objects with thermal properties, while the billet was selected as a deformable object with thermal properties. The tools were meshed with different sizes and a uniform mesh set was stablished for the billet. The tools were meshed by 2D triangular elements, and the Cr13 steel billet was meshed by 3D tetrahedral P1+ linear elements. The length of the initial billet was set to 600 mm. For reporting simulation results, two views were selected, one from upside (without upper roller) and another from side view (without Diescher). The schematic view of the selected view for simulation results is shown in Fig. 1c.

2.3. Constitutive models

In this study, super Cr13 martensitic stainless steel (MSS) has been selected as base metal (billet). The chemical composition of the billet is presented in Table 1. Hansel-Spittel constitutive law was chosen to model Cr13 MSS behavior at different temperatures, strain, and strain rates. The material was tested at different temperature (900°C–1250 °C) and strain rate

Table 1 – Chemical composition of Cr13 MSS.

Element	C	Cr	Ni	Mn	Si	Mo	P	S	Ti	V	Fe
Wt.%	0.03	11.5–13.5	4.5–6.5	0.5	0.5	1.5–3	0.03	0.005	0.01–0.5	0.5	Bal

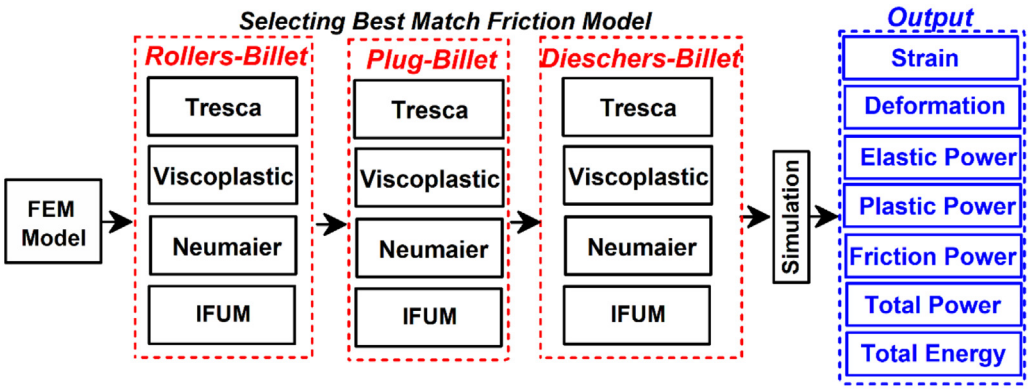

Fig. 2 – Used procedure for selecting different contact and friction situation between tools and billet.

($0.05s^{-1}$-$10s^{-1}$) experimentally. The flow stress curves were used to adjust the constitutive law by fitting approach and afterwards, it was exported to the materials library of FORGE® NxT. These numbers are used to ensure the reliability of FEM results during the simulation process. The example of used flow curve in $0.05s^{-1}$ and $10s^{-1}$ strain rate depicted in Fig. 1d and e, respectively.

2.4. *Contact and friction model*

First, the friction model for rollers-billet, plug-billet, and Diescher disks-billet interfaces was investigated. The contact between the Thrust Bench and Guide billet was selected without friction. In this step, various friction models are implemented on the tools–billet interfaces. Those friction models already used in the simulation of TPP were selected [15]. Accordingly, Tresca, Viscoplastic, Neumaier, and IFUM friction models were considered. The friction models were set at rollers-billet, plug-billet, and Diescher disks-billet interfaces. The step by step chart for friction model selection is presented in Fig. 2. After several simulation tests and comparisons with experimental results, the best friction model for each contact area was selected. The viscoplastic friction model was selected for rollers and billet, and the Tresca model was selected for the other contact areas. In the next step, various friction coefficients were selected to find the effects of friction on total energy consumption. The friction coefficient range at the roller-billet (RF) interface was 0.1–0.6, the friction coefficient range at the plug-billet (PF) interface was 0.06–0.15, and the friction coefficient range at the Diescher disks-billet (DF) interface was

Table 2 – Simulation plan.

Sample Number	Roller–Billet Contact area (Viscoplastic friction Model)	Diescher–Billet Contact area (Tresca friction Model)	Plug–Billet Contact area (Tresca friction Model)
	Friction Coefficient	Friction Coefficient	Friction Coefficient
1	0.1	0.06	0.2
2	0.1	0.1	0.2
3	0.1	0.15	0.2
4	0.2	0.06	0.2
5	0.2	0.1	0.2
6	0.2	0.15	0.2
7	0.3	0.06	0.2
8	0.3	0.1	0.2
9	0.3	0.15	0.2
10	0.4	0.06	0.2
11	0.4	0.1	0.2
12	0.4	0.15	0.2
13	0.5	0.06	0.1
14	0.5	0.06	0.2
15	0.5	0.06	0.3
16	0.5	0.1	0.1
17	0.5	0.1	0.2
18	0.5	0.1	0.3
19	0.5	0.15	0.1
20	0.5	0.15	0.2
21	0.5	0.15	0.3
22	0.6	0.06	0.2
23	0.6	0.1	0.2
24	0.6	0.15	0.2

0.1–0.3, respectively. These numbers were selected according to the available tests on the actual situation in the industry [16]. Table 2 presents the friction models at interfaces and friction coefficient ranges for all interfaces used during simulation of TPP, and the resulting models analyzed.

3. Experimental procedure

At the early stage, the billet of Cr13 MSS is heated up until 1250 °C in a furnace for 120 min. The hot billet has no pierce or holes. After that, the hot billet is transferred to a specific chamber (Phase (I)). A thrust bench pushes forward the hot billet into the main tooling box in the chamber. The hot billet passes through the Guide and contacts the rotational rollers. There are two rollers that rotate and push the billet forward by friction. The rotational advance movement of the billet leads the generation of the hollow cavity by the plug (Phase (II)). During the piercing phase, two Diescher disks control the geometry of the tube in order to remove any twisting and eccentricity. During piercing, the length of the billet increases, and the thickness of tube walls decreases. In this setup, the plug cannot move in X, Y, or Z direction, but the Plug can freely rotate. At the end of this stage, the final tube is produced (Phase (III)). The picture of TPP phases is depicted in Fig. 3a. The Process parameters, geometrical issues, and wall thickness are not the aim of this study. For this reason, these points are ignored. In order to find the minimum energy consumption, the electricity consumption by rollers was recorded in real situation and reported as total energy consumption (Fig. 3b). The recorded data is used for validation of FEM simulation results. The geometry of tools and billet and kinematics of tools was set according to the details described in Section 2.1. The production of tube and energy issues was the main factors considered in this study.

4. Results and discussions

4.1. *Effects of friction coefficient on tube geometry and stain*

In TPP, the billet is first pushed by the bench and, after contacting with the rollers, the billet diameter reduction starts. After that, the billet contacts with the plug and the piercing starts. Consequently, the piercing plug force is increased, and the forward velocity of the workpiece drops. From this moment, the tube elongation and the reduction of its cross

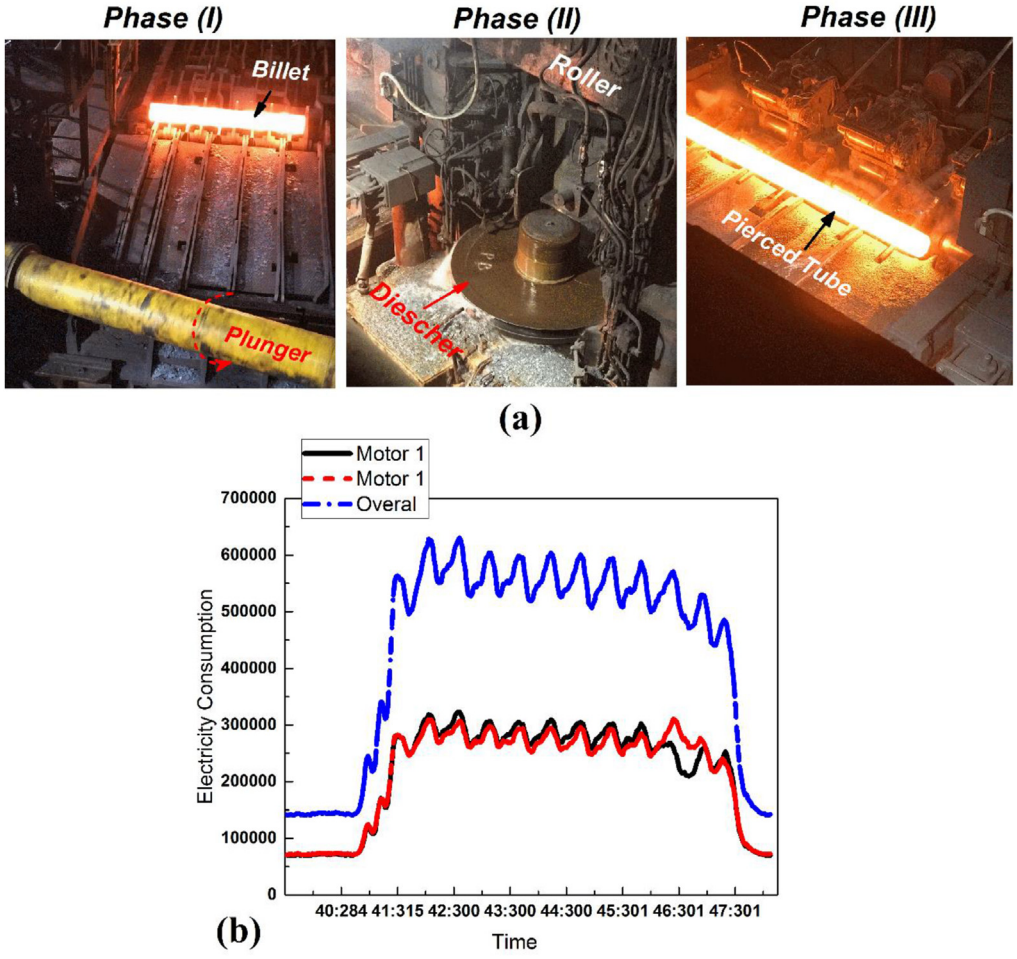

Fig. 3 – (a) Various phase of piercing process and (b) Recorded electricity usage of roller 1 (motor 1) and roller 2 (motor 2) during piercing process.

section begins. In the next step, the steady-state phase of starts until the end of the process. In the meantime, the role of Diescher disks is to control the produced geometry and help to forward-moving of billet.

In Fig. 4, shows the different contact areas between tools and billet for sample 14. As it can be seen the bigger contact areas correspond to the contact of the billet with the rollers and the billet with the plug. Consequently, friction at rollers and friction on the plug play a prominent role during the piercing process. On the other hand, due to the small contact area between Dieshers and billet, the effects of Dieshers on moving forward of the tube are not significant. The critical issue during TPP is the finishing piercing phase. Generally, the contact condition is local and, during the process, it is tough to find the exact contact area between tools and billet. The surface contact area between Roller–Billet and Diescher–Billet at the first step of complete contact and steady-state is depicted in Figs. 4a and b, respectively. As seen, the contact area at the different stages is not the same. This contact behavior is similar in the Plug-billet contact area (Figs. 4c and d). The overall conclusion in contact issues could be the difference between areas and tools mentioned before. The first point to analyze of the selected friction coefficient between roller and workpieces, is to check if all friction conditions conclude to produce sound tube or not. In this regard, the simulation results revealed that the piercing process is not finished for a value of friction coefficient of 0.1 in the Rollers-billet contact (samples 1, 2 and 3) as it can be seen in Fig. 5a. Accordingly, the piercing process is completely formed at roller friction coefficients above 0.1. Fig. 5b and c presents the pierced tube at 0.3 (sample 7) and 0.5 (sample 14) friction coefficients at Roller–Billet interface. According to simulation results, at low friction coefficient values, such as 0.1, the friction driving force generated between rollers and workpiece is not big enough to overcome plug resistance force, and the tooling system is not able to finish the piercing process. On the other hand, the friction coefficient at Plug-billet interface does not have a significant effect compared to Roller–Billet friction coefficient. The pierced tube with friction coefficient of 0.5 at Roller–Billet interface and Plug–Billet friction coefficient of 0.1, 0.2 and 0.3 (samples 13, 14 and 15) are depicted in Figs. 5d, e and 5f, respectively. As shown, all tubes are pierced properly and without any defect. The statistical results of pierced tubes are presented in Fig. 5g and h. The results reveal that the friction coefficient directly affects the length of final product. The geometrical dimension of produced tubes at various friction coefficient shows that, with increasing Roller–Billet friction coefficient, the length of pierced tube decreases. Thus, the increase of friction at roller-billet interface reduces the length of final tube. Similarly, increasing friction coefficient at Plug–Billet interface leads to a decrease of the tube length. The analysis of the results shows that, the Roller–Billet friction coefficient presents bigger effects on tube length compared to Plug–Billet friction coefficient.

For example, the tube corresponding to Sample 14 was near 80 mm shorter than the one of Sample 4. On the other hand, by increasing the friction coefficient at the Diescher–Billet interface, the length of the final tube moderately decreases.

The simulation results of strain at various friction coefficients are depicted in Fig. 6. According to simulation output, the relation of friction coefficients and tube length is almost repeated in strain results. Apart from the tube piercing process that was uncompleted at samples 1, 2, and 3, the strain on other samples shows that the strain of tube decreases with increasing RF friction coefficient.

The simulation results of strain can be divided into two groups. First, the surface strain at the interfaces of tools and super Cr13 steel billet. Second, the strain of other parts of the

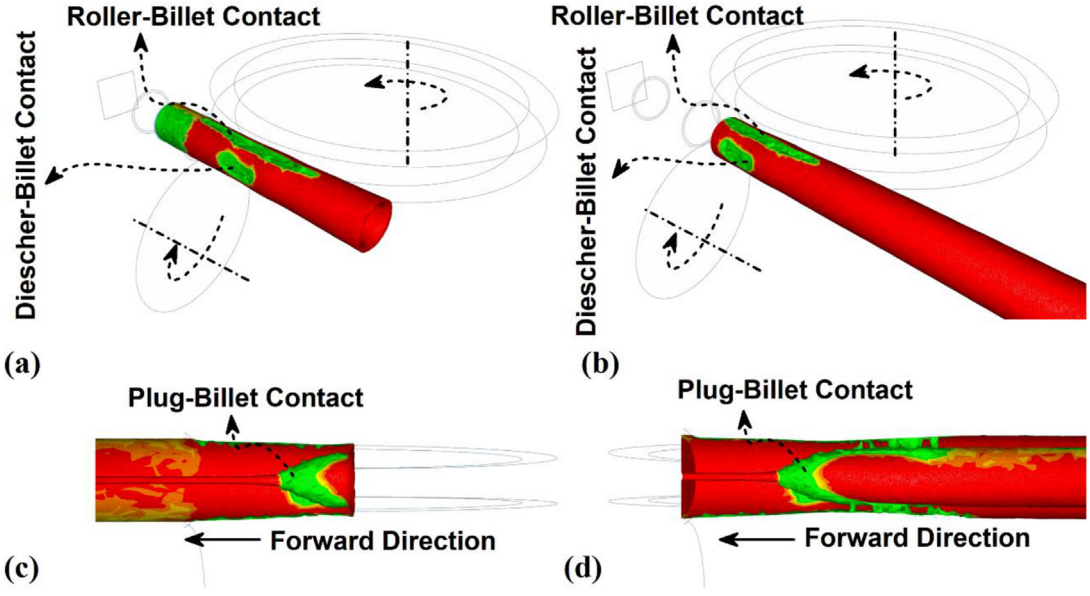

Fig. 4 – Contact area (green zone) between Roller–Billet and Diescher-billet at (a) early stage and (b) steady state of piercing process. Contact area (green zone) between Plug–Billet at (a) early stage and (b) steady state of piercing process.

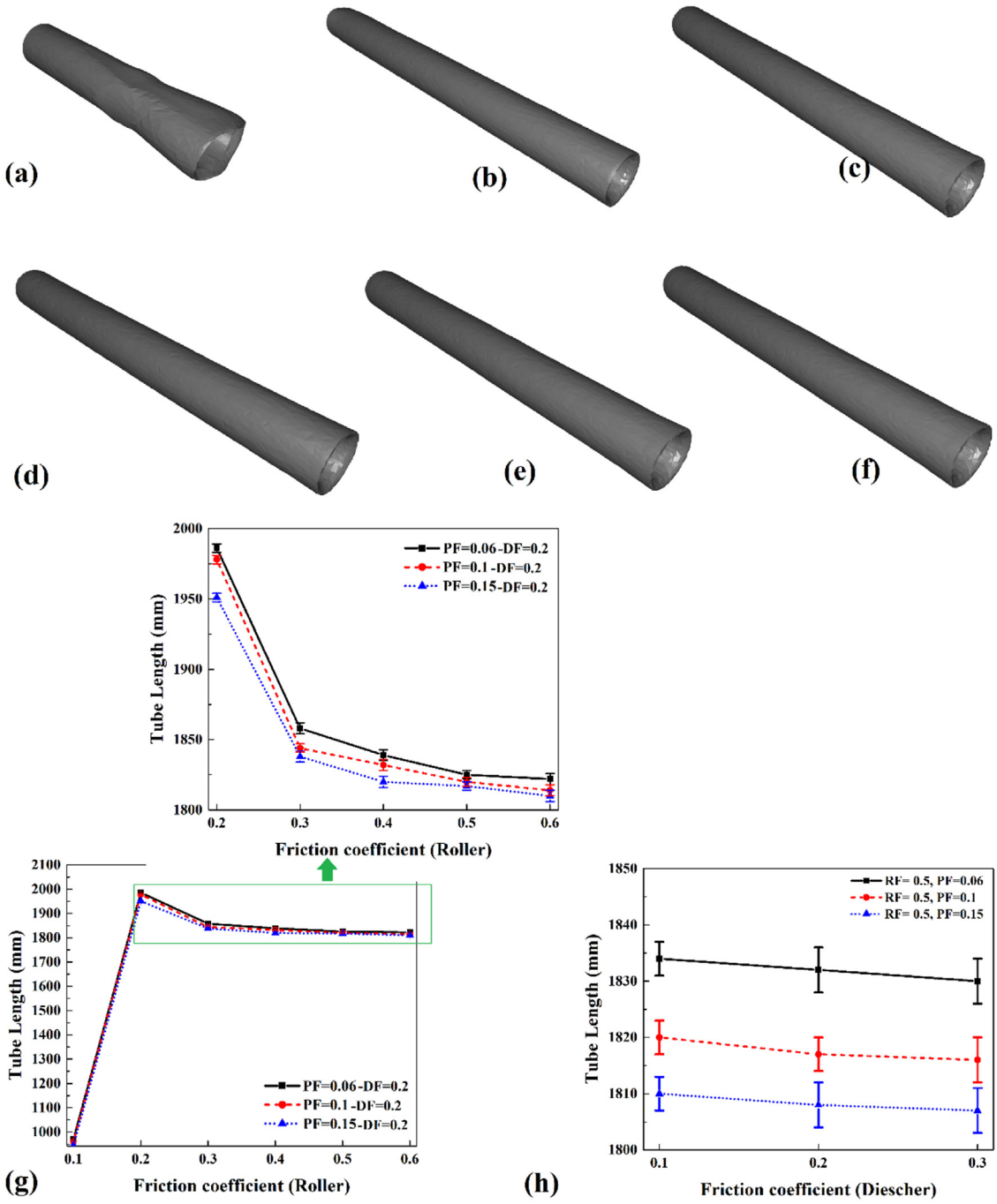

Fig. 5 – Simulation results of pierced tube length of (a) Sample 1, (b) Sample 4 and (c) Sample 14. Simulation results of pierced tube length of (d) Sample 13, (e) Sample 14 and (f) Sample 15. (g) Relation RF and PF on pierced tube length. (h) Relation DF on pierced tube length.

tube after deformation. The simulation results of strain at interfaces are local and, in this section, the average tube strain is reported. This average number indicates the strain of super Cr13 steel billet from the starting to the ending of the piercing process. It can be seen that the strain of the tube decreases with increasing PF friction coefficient. The simulation results of strain on tubes of samples 1 and 14 are depicted in Figs. 6a and b, respectively. On the other hand, the strain in the internal section of the tube sample 14 is depicted in Fig. 6c. According to the obtained results, the strain can locally change. As it can be seen in Fig. 6c, strain is progressively increased as long as the area of the tube cross section is reduced. The sided view of samples 13 and 15 pierced by different friction conditions at DF interface is depicted in Figs. 6d and e, respectively. The results revealed that the friction at DF does not significantly affect strain and tube length. The highest strain was recorded in RF = 0.2, and therefore, the tubes formed with this friction coefficient were longer than

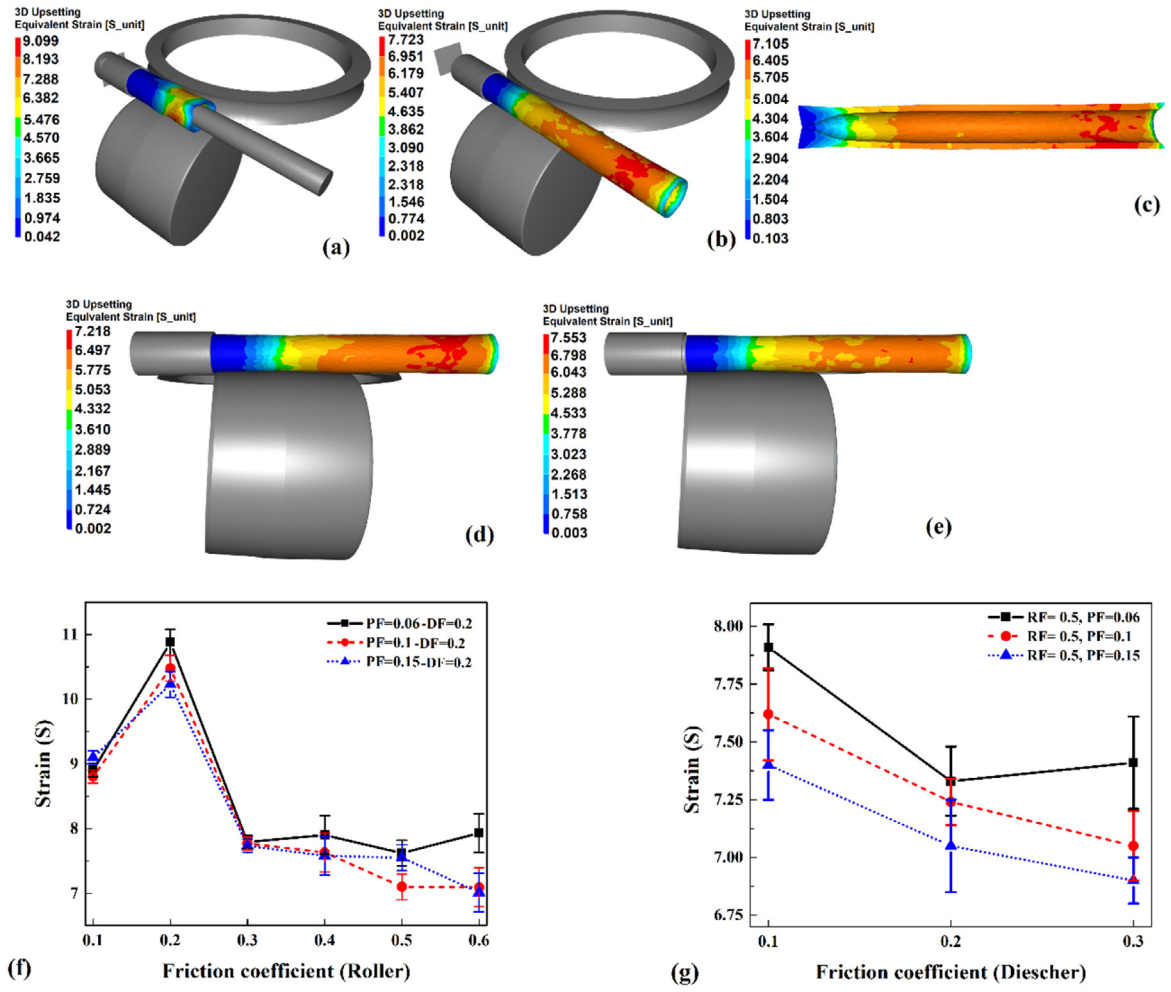

Fig. 6 – Simulation results of pierced tube strain of (a) Sample 1, (b) Sample 4 and (c) Sample 14. Simulation results of pierced tube strain of (d) Sample 13, (e) Sample 15. (f) Relation RF and PF on pierced tube strain. (g) Relation DF on pierced tube strain.

other produced tubes. The statistical results showing the effect on the strain of the friction coefficient at various interfaces is depicted in Figs. 6f and g. As the results show, the strain decreases with increasing friction at RF and PF. The highest strain was simulated with RF = 0.2 and lowest value was predicted with RF = 0.6. On the other hand, the effects of friction at DF were not significant on the strain of the tube. As a survey, it can be seen that with increasing DF, the strain of the pierced tube slightly decreases.

4.2. *Effect of friction condition on normal stress*

Fig. 7 displays the simulation results of normal stress on the high-pressure contact zone between billet and tools. Tools apply the normal stress at contact areas. For this reason, the friction coefficient can affect the normal stress distribution on the tube during the Piercing process [17]. Due to the tilted angle of the rollers, the contact area between rollers and billet is not straight—this contact type (between rollers and billet) is known as well ¨non-uniform cross roll surface statë [18]. Obtained results show that the stress concentration zone is the contact area between rollers and Cr13 steel billet.

Consequently, the highest stress is predicted in this area by the simulations. The simulation results of normal stress on the tube with RF = 0.1 (Sample 1), 0.3 (Sample 7), and 0.5 (Sample 14) are shown in Figs. 7a, b, and 7c, respectively. The results show that with increasing RF friction coefficient, the surface stress decreases. The sign of normal stress is negative, which means compression stress. As results revealed, the normal stress starts to grow on the billet after the straight contact with the roller. It seems that both the time and contact type can affect normal stress. In the piercing phase, the normal stress is a dynamic contact and, with higher RF, the contact time decreases. Consequently, the normal stress on the surface tends to decrease [19]. On the other hand, the PF affects normal internal stress. As discussed before, the normal stress is high in the contact area between tools and workpiece. Normal stress in the interior of sample 14 is depicted in Fig. 7d. Figure 7e and Fig. 7f show the normal stress of sample 17 and sample 20, respectively. The aim of selecting samples 17 and 20 was the evaluation of the effects of friction at DF on normal stress. As the results show, DF friction effect on normal stress is not as intense as those of RF and PF, but increasing DF friction increases normal stress. To better understand friction

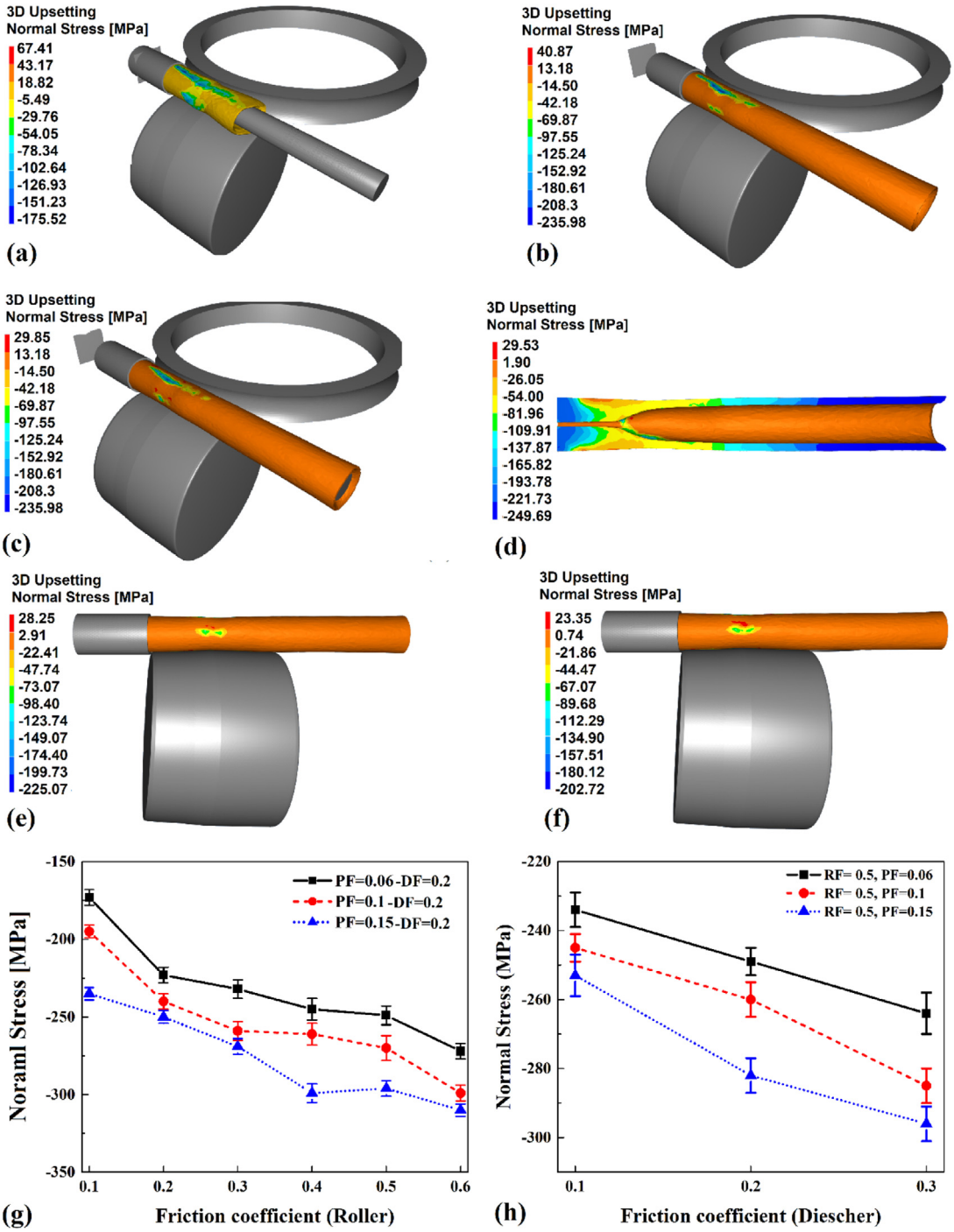

Fig. 7 – Simulation results of pierced tube Normal Stress of (a) Sample 1, (b) Sample 7 and (c) Sample 14. Simulation results of pierced tube Normal Stress of (d) Sample 13, (e) Sample 15. (f) Relation RF and PF on pierced tube Normal Stress. (g) Relation DF on pierced tube Normal Stress.

coefficient effects, the average normal stress of the billet is presented in Figs. 7g and f. The trend of friction at RF and PF depicted in Fig. 7g reveals that, with increasing friction coefficient at RF and PF, the absolute value of normal stress is increased. For example, the absolute value of average normal stress of sample 4 (~-220 MPa) shows an increase of 22 MPa in sample 6 (~-242 MPa). This trend evidences the effects of increasing friction at PF on normal stress. The trend is similar to what can be appreciated in all friction conditions for RF interface. Results show that with increasing friction at RF interface, the absolute value of normal stress increased slightly.

For example, the absolute value of average normal stress at sample 4 (~-220 MPa) shows a difference of 40 MPa with respect to sample 22 (~-260 MPa). On the other hand, as discussed before, due to the lower contact area existing between

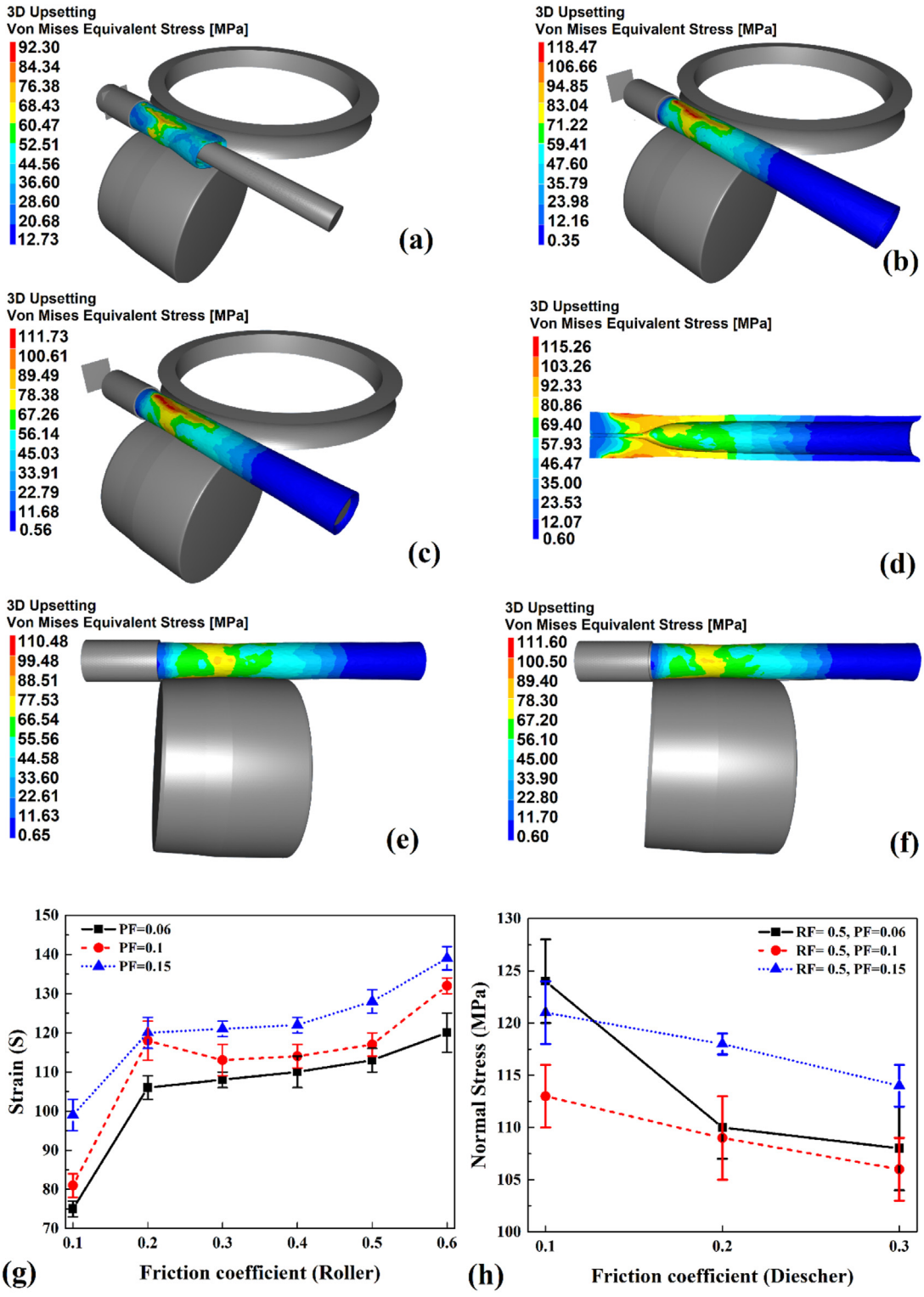

Fig. 8 – Simulation results of pierced tube Von-Mises equivalent stress of (a) Sample 1, (b) Sample 7 and (c) Sample 14. Simulation results of pierced tube Von-Mises equivalent stress of (d) Sample 13, (e) Sample 15. (f) Relation RF and PF on pierced tube Von-Mises equivalent stress. (g) Relation RF and (h) DF on pierced tube Von-Mises equivalent stress.

Dieschers and billet, increasing friction in this area does not have a significant impact on normal stress. Fig. 8 shows Von-Mises equivalent stress on the billet's surface during the piercing operation presenting the same trend as the one described in Fig. 7. Results from Von-Mises equivalent stress on the tube with RF = 0.1 (Sample 1), 0.3 (Sample 7), and 0.5 (Sample 14) are shown in Figs. 8a, b, and 8c, respectively, showing and increase of Von-Mises equivalent stress with

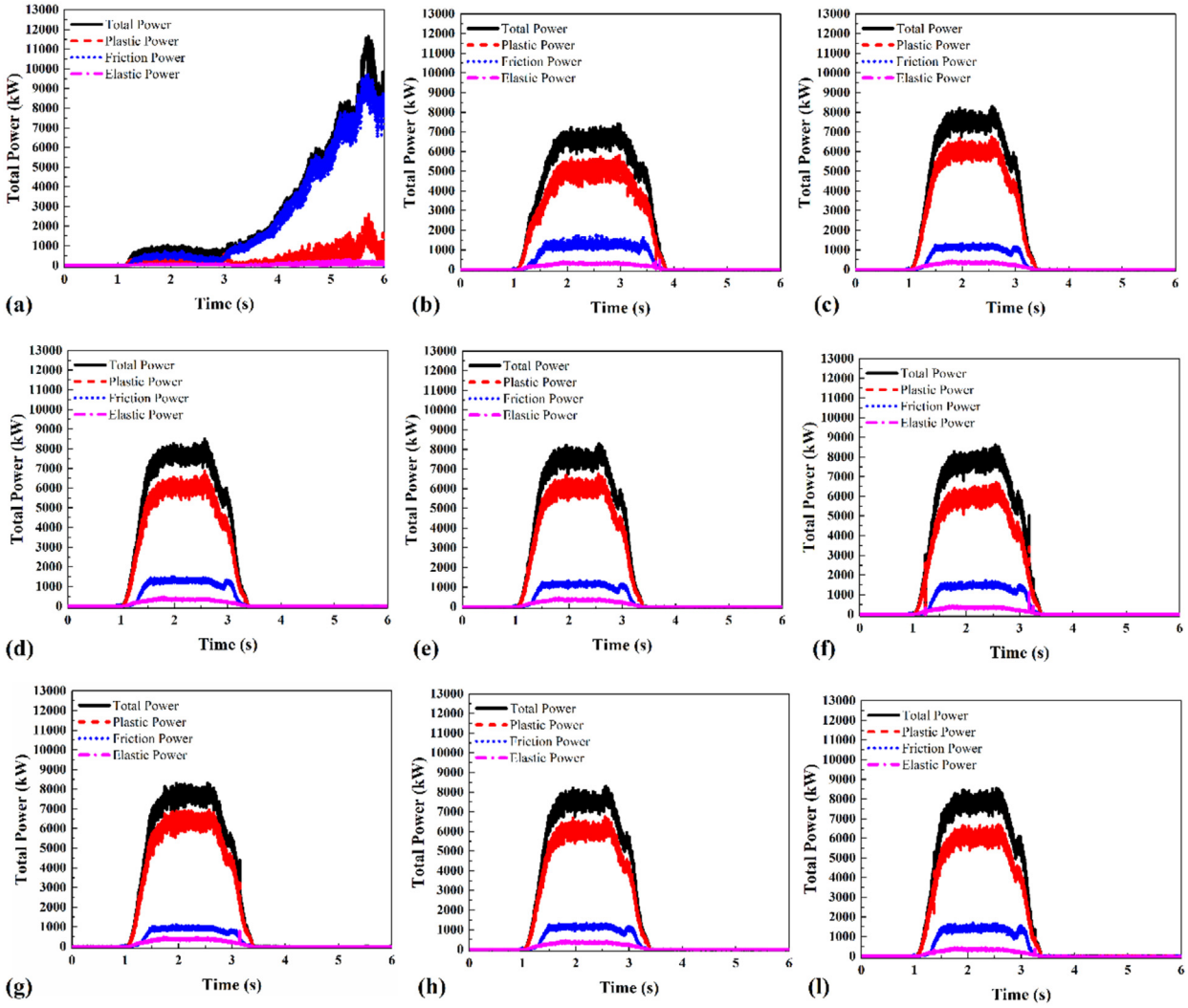

Fig. 9 – Simulation results of total power in piercing process sample (a) 1, (b) 4, (c) 17, (d) 14, (e) 17, (f) 20, (g) 13, (h) 14, and (i) 15.

increasing RF friction factor. Fig. 8d shows the Von-Mises equivalent stress inside sample 14, and Fig. 8e and f shows the Von-Mises equivalent stress of sample 17 and sample 20, respectively. The relation between Von-Mises equivalent stress and the friction coefficient is shown in Figs. 8g and h. Regarding Von-Mises equivalent stress, the trend is similar to the one of normal stress, with a positive sign.

4.3. *Effects of friction coefficient on total power*

The total power is defined by the sum of the power dissipated by elastic deformation, plastic deformation, and friction. For this reason, the study of the different parts of the total power provides valuable information. In this section, the effect of friction at RF, PF and DF interfaces is studied by means of case samples and generic results. Figs. 9a, b and 9c show the elastic (power dissipated by elastic strain), plastic (power dissipated by plastic strain), friction (power dissipated by friction) and total power of Sample 1, Sample 7 and Sample 14, respectively.

These samples are selected to analyze the effect of friction at RF on total power. In RF = 0.1 (sample 1) case, the results show that the elastic and friction powers are very low, while the plastic power, in this case, is high. From the obtained results, it is revealed that the case with low friction coefficient (RF = 0.1) was not able to finish piercing process. It seems that in this case the contact situation in rollers-billet interface is pure sliding and the rollers are not able to push forward the billet. The power trend for friction coefficient values higher than 0.1 at RF changes.

The results from RF = 0.3 (Sample 7) indicates that elastic and plastic powers increase, while friction power decreases. The difference between plastic power and friction power in RF = 0.2 is lower than in other cases. With increasing friction coefficient at RF interface, the power dissipated by plastic strain is increased (sample 14). The effects of friction at PF on total power are presented in Figs. 9d, e and 9f, which show the results that correspond to samples 14, 17 and 20, respectively. The trend shows that with increasing friction at PF total power is also increased. The total power of samples 13, 14 and 15, pierced with DF = 0.1, DF = 0.2 and DF = 0.3, is presented in Figs. 9g, h and 9f. The results reveal that friction at DF does not significantly affect the total power consumption. To better

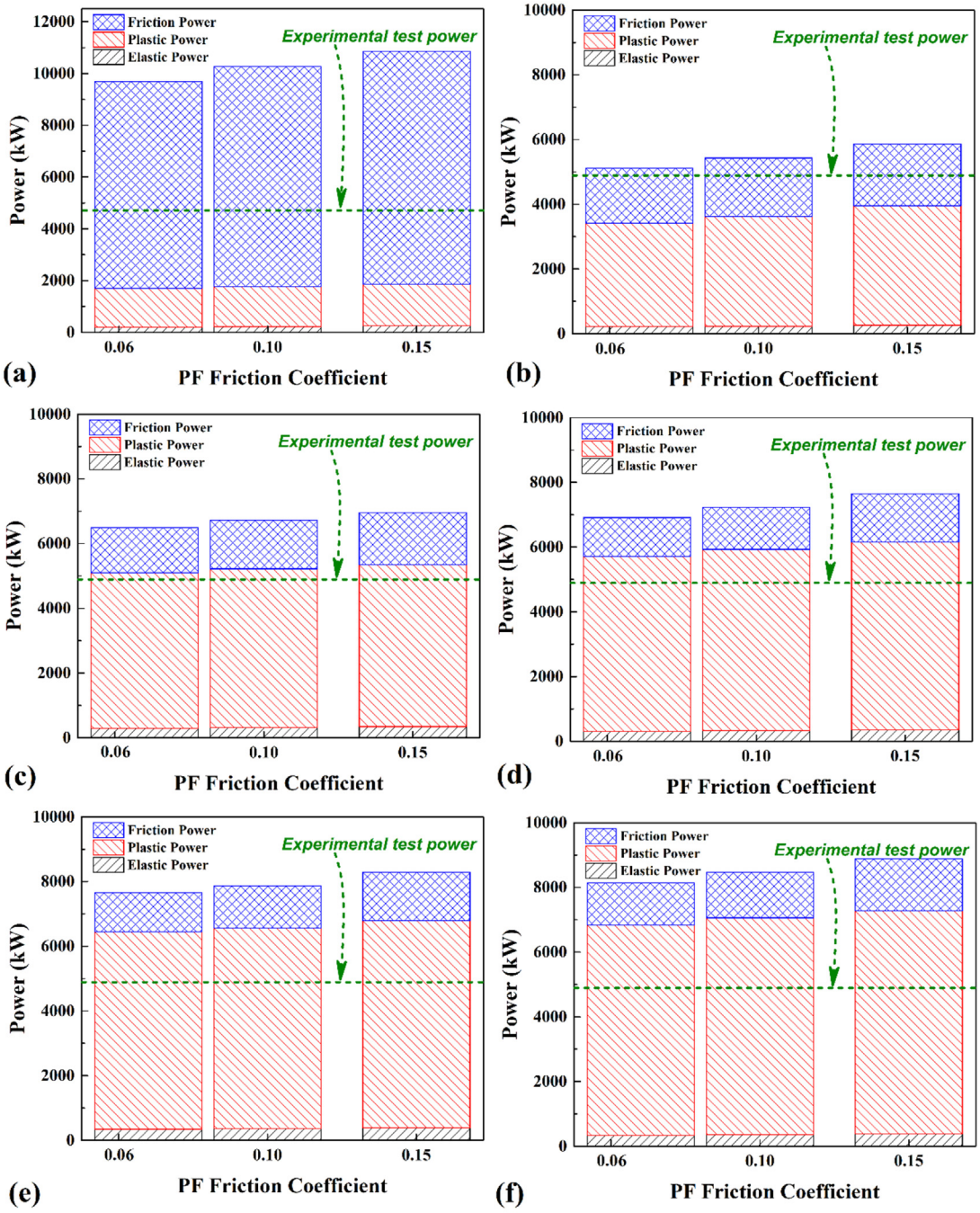

Fig. 10 – Simulation results of total power in piercing process with RF (a) 0.1, (b) 0.2, (c) 0.3, (d) 0.4, (e) 0.5 and (f) 0.6.

understand all details about total power, the statistical results of different friction coefficients are depicted in Fig. 10.

Elastic, plastic, friction, and total power of pierced samples classified by different DF and RF are gathered. Results show that a higher friction coefficient sticking at the interface of rollers and billet increases the plastic deformation of super Cr13 steel. In other words, the lower friction leads to sliding contact between rollers and billet, while higher friction leads to sticking-sliding contact. Apart from those cases in which RF = 0.1, the friction power decreases by increasing RF. On the other hand, by increasing PF, the friction power increases. The elastic power and plastic power increase both with increasing RF and increasing PF. The sum of elastic, plastic, and friction power provides the total power of the piercing phase, and in Fig. 10 the total power of experimental tests is depicted by the green dash-line. According to the experimental records, the simulated case that better matches experimental total power is sample 4.

The simulation results revealed that the minimum total power consumption corresponds to RF = 0.2, while the maximum power is consumed at RF = 0.6. On the other hand, among various PF friction conditions, the minimum total power is produced at PF = 0.06 and maximum at PF = 0.15. The trend of powers in sample 4 (RF = 0.2, PF = 0.06) and sample 6

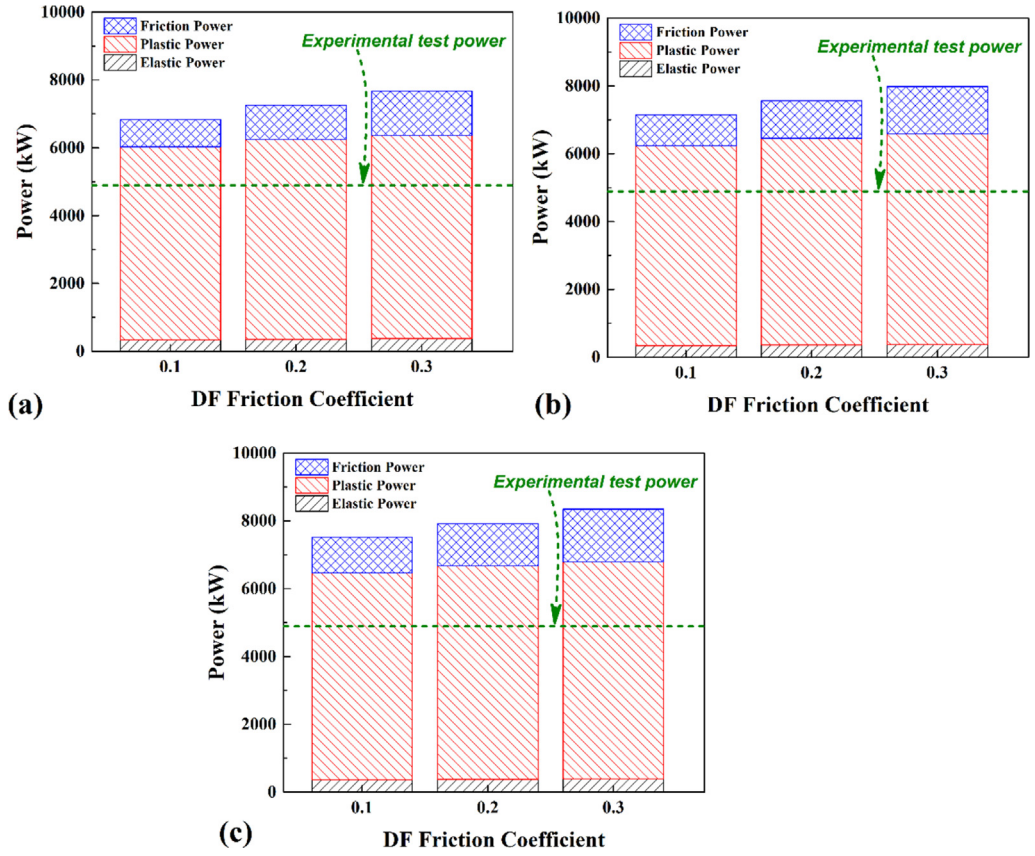

Fig. 11 – Simulation results of total power in piercing process sample of various DF, RF = 0.5 and (a) PF = 0.06, (b) PF = 0.1 and (c) PF = 0.15.

(RF = 0.2, PF = 0.15) reveal that the elastic power increased from 220kw to 260kw, plastic power increased from 3200kw to 3700kw, and friction power increased from 1700kw to 1900kw. The trend of samples 22 (RF = 0.6, PF = 0.06) and sample 24 (RF = 0.6, PF = 0.15) revealed that elastic power increased from 340kw to 365kw, plastic power increased from 6500kw to 6900kw, and friction power increased from 1300kw to 1600kw. The simulation results which show the effects of different friction conditions at DF on total power are presented in Fig. 11. According to the results, the total power is increased by increasing friction at DF, but the impact of friction at DF on total power is not as significant as friction at RF for super Cr13 stainless-steel. The statistical analysis of results reveals that all elastic, plastic and friction powers increase with increasing friction at DR interface. The highest power is produced at DF = 0.3, while the lowest is produced at DF = 0.1. The simulation results of power in sample 13 (RF = 0.5, PF = 0.06, DF = 0.1) and sample 15 (RF = 0.2, PF = 0.15, DF = 0.3) show that the elastic power increases from 330kw to 370kw, plastic power increases from 5700kw to 6000kw, and friction power increases from 800kw to 1300kw. The trend of samples 19 (RF = 0.5, PF = 0.06, DF = 0.1) and 21 (RF = 0.5, PF = 0.06, DF = 0.3) reveals that elastic power increases from 365kw to 395kw, plastic power increases from 6100kw to 6400kw, and friction power is increased from 1050kw to 1550kw.

As discussed before at RF = 0.1, the friction at the roll-billet critical contact is not high enough to push the billet forward. For this reason, the energy consumption at RF = 0.1 is higher than in other cases, but the tube is not formed. With increasing friction coefficient at RF interface, the total period of process decreases. Consequently, the minimum friction coefficient to finish the piercing process is RF = 0.2. The simulation results reveal that the piercing process time are shorter for higher friction at RF, while they are larger for higher friction at PF.

It can be concluded that the material strain rate decreases with a higher friction coefficient at the plug interface. It means that the resistance against moving forward of super Cr13 steel increases with higher friction at PF interface. As mentioned before, the higher friction coefficient at the plug-billet interface also decreases plastic deformation power during the piercing phase. The statistical data of process time at various friction conditions at RF with PF = 0.06, PF = 0.1, and PF = 0.15, is presented in Figs. 12a, b and 12c, respectively. According to the simulation results, the piercing time finds a stable trend after RF = 0.5 and the difference between RF = 0.5 and RF = 0.6 in all PF conditions is very small. The results indicate that the shortest piercing process can be achieved at RF = 0.6 and PF = 0.06. The simulation results also reveal that the piercing process at sample 4 (RF = 0.2, PF = 0.06) is finished after ~4s, while the piercing process at sample 6 (RF = 0.2, PF = 0.15) is finished after ~4.4s. Furthermore, results indicate that piercing process at sample 22 (RF = 0.5, PF = 0.06) is finished ~3.2s, while the piercing process at sample 24 (RF = 0.5, PF = 0.15) is finished ~3.5s. The effects of various friction conditions at DF are depicted in Figs. 12d, e, and 12c. The main output from these results is that, with increasing friction at

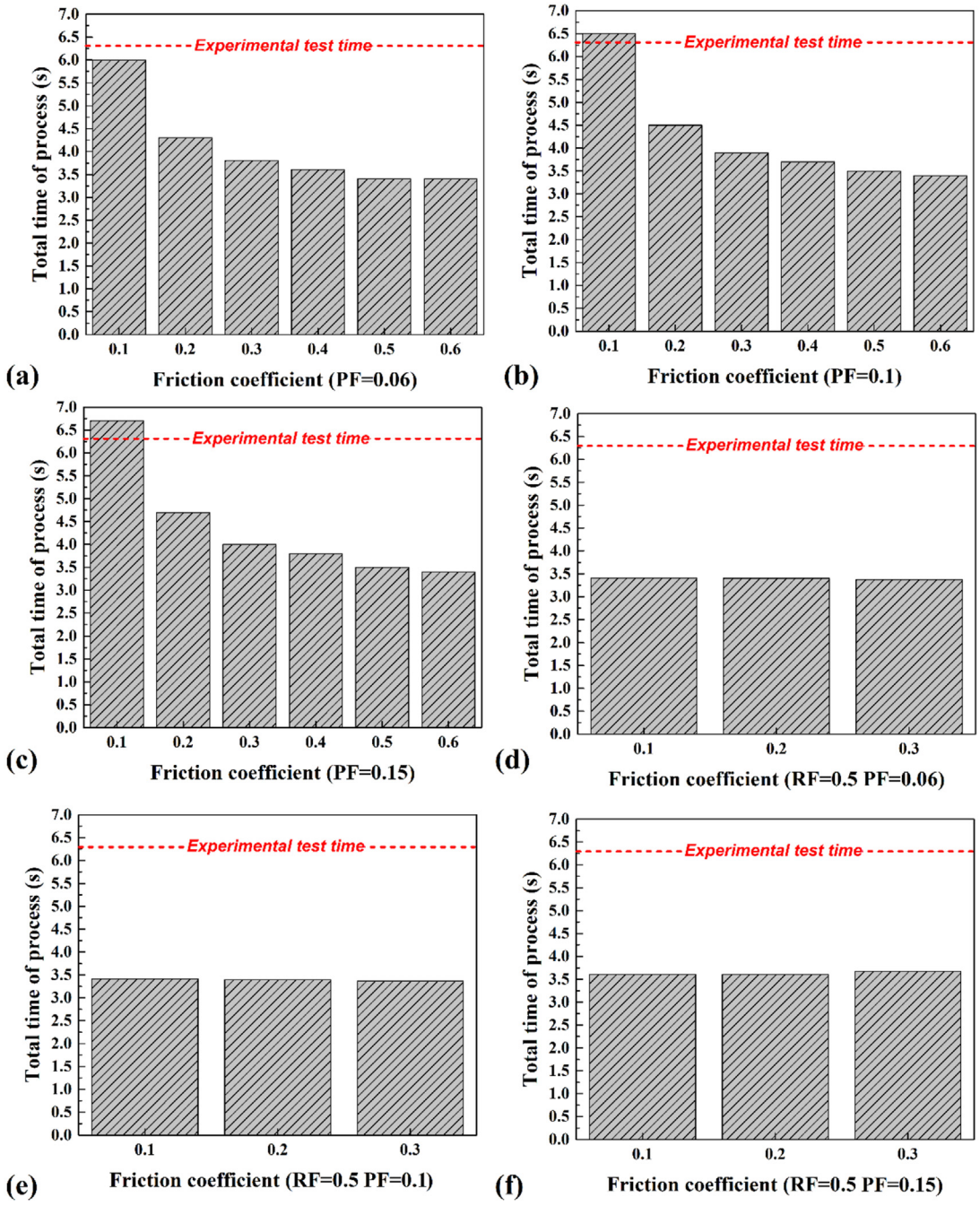

Fig. 12 – Simulation results of time in piercing process of various RF and (a) PF = 0.06, (b) PF = 0.1 and (c) PF = 0.15. Simulation results of time in piercing process of various DF and (a) PF = 0.06, (b) PF = 0.1 and (c) PF = 0.15.

DR, the piercing time delay slightly increases. The simulation results of samples 19 (RF = 0.5, PF = 0.06, DF = 0.1) and sample 21 (RF = 0.5, PF = 0.06, DF = 0.3) indicated that the piercing process time would be 3.41s and 3.37s, respectively.

4.4. *Effects of friction coefficient on total energy*

One of the main parameters during the piercing phase is calculating total energy usage during manufacturing.

From the results of total power during the piercing stage, the total amount of energy consumption can be estimated. In this research, the simulation results revealed that the friction coefficient at interfaces of tooling and billet could change the total piercing time and total power. Thus, these results prove that the friction coefficient can change the energy consumption required for tube piercing. The statistical results of energy consumption at different friction conditions at RF, PF, and DF are shown in Fig. 13. The energy consumption result for various friction conditions at RF, with PF = 0.06, PF = 0.1, and PF = 0.15, is presented in Figs. 13a, b, and 13c, respectively.

Contrary to the trend of total power, the energy consumption decreases with increasing friction at RF. As it can be

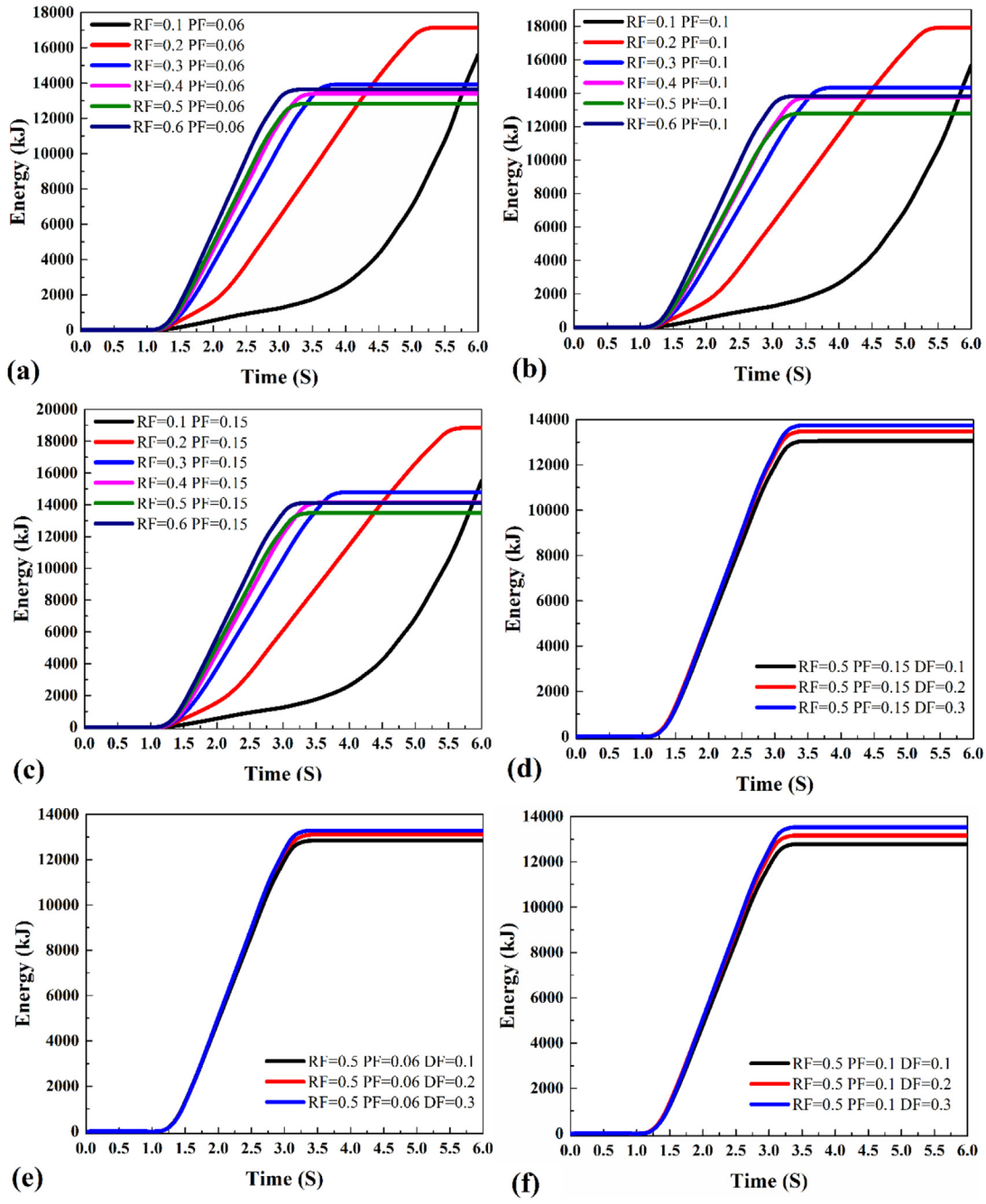

Fig. 13 – Simulation results of total energy consumption in piercing process of various RF and (a) PF = 0.06, (b) PF = 0.1 and (c) PF = 0.15. Simulation results of total energy consumption in piercing process of various DF and (a) PF = 0.06, (b) PF = 0.1 and (c) PF = 0.15.

observed in Fig. 13, energy consumption decreases as long as RF coefficient is increased from 0.1 to 0.5, while it rises for RF values above 0.5. However, the effects of friction at PF are similar to those of total power. With increasing PF, the energy consumption was increased in all cases. The results show that the total energy in the pierced tube with PF = 0.06 decreased from 17300 kJ (RF = 0.2) to 12800 kJ in the RF = 0.5 sample and, after that, increased to 13700 kJ at RF = 0.6. This trend was detected in the pierced tube with PF = 0.15 as well. According to the results in PF = 0.15, the total energy decreased from 18800 kJ (RF = 0.2) to 13400 kJ in the RF = 0.5 sample and increased to 14300 kJ at RF = 0.6. The investigation on the effects of friction at DF on total energy shows that the minimum energy consumption was recorded at DF = 0.1, while the maximum was recorded at DF = 0.3. The result of energy consumption at RF = 0.5, PF = 0.06 revealed that the total energy consumption was increased from 12600 kJ at DF = 0.1–12900 kJ at DF = 0.3. Similarly, regarding energy consumption at RF = 0.5, PF = 0.15, it shows an increase from 13100 kJ at DF = 0.1–13550 kJ at DF = 0.3.

5. Conclusion

In this research, a tube piercing process at high temperature was successfully simulated by FEM. The super Cr13 Stainless-steel is used as a billet. Various friction coefficients were selected at tools–billet interfaces. The relation between friction coefficients and produced tube length, stress, total power, and energy consumption was investigated and from the results, the following conclusions are drawn:

1 The results revealed that the contact area between tools and billet changes with friction coefficient. Generally, high friction coefficients lead to higher contact area. A higher contact area between tools and billet leads to an increase of both, the strain of the tube and its length. According to the obtained results, the longest tube is produced at RF = 0.2, PF = 0.06 and DF = 0.1 with 1980 mm, while the shortest tube is produced at RF = 0.9, PF = 0.15, and DF = 0.3 with 1810 mm.
2 The surface normal stress increases in rollers-billet and Dieschers-billet interfaces by increasing friction at RF and DF. Furthermore, the normal internal stress at the plug-billet interface increases with increasing friction at PF. The results revealed that the minimum compression stress increases from 220 MPa at RF = 0.2, PF = 0.06, and DF = 0.1–260 MPa at RF = 0.5, PF = 0.15, and DF = 0.3.
3 The total power during the piercing process consists of Elastic, Plastic, and friction powers. The results show that total power increases with increasing friction coefficient at interfaces. The detailed information revealed that with increasing friction at RF and PF, both the elastic and plastic powers increased, while friction power decreased.
4 The results revealed that with increasing friction coefficient, tube deformation increased, and RF's main effects are controlling tube geometry. The results indicated that tube with highest length was produced at RF = 0.2, while the shortest was produced at RF = 0.6. Then, friction conditions at PF and DF present a lower impact on produced final tube compared to those at RF.
5 The study of energy consumption revealed that the optimum energy consumption could be obtained with FR = 0.5, PF = 0.06, and DF = 0.3. In this situation, the consumed energy for the tube piercing process is 12600 kJ.

Declaration of Competing Interest

The authors declare that they have no known competing financial interests or personal relationships that could have appeared to influence the work reported in this paper.

Acknowledgement

This project has received funding from the European Union's Horizon 2020 Research and Innovation Programme under the Marie Skłodowska-Curie grant agreement No. 847624. In addition, a number of institutions back and co-finance this project. The paper reflects only the authors' view and the Agency is not responsible for any use that may be made of the information it contains.

REFERENCES

[1] Fernandes M, Marouf N, Montmitonnet P, Mocellin K. Identifying heterogeneous friction coefficients on the hot forming tools in Mannesmann cross-roll piercing. Defect Diffusion Forum 2022;414:117–23. https://doi.org/10.4028/p-xg657s.
[2] Brensing K-H, Großrohre S. Steel tube and pipe manufacturing processes. 2004.
[3] Murillo-Marrodán A, García E, Barco J, Cortés F. Analysis of wall thickness eccentricity in the rotary tube piercing process using a strain correlated FE model. Met 2020:10.
[4] Murillo-Marrodán A, García E, Barco J, Cortés F. Application of an incremental constitutive model for the FE analysis of material dynamic restoration in the rotary tube piercing process. Mater 2020;13.
[5] Zhang Z, Liu D, Yang Y, Zheng Y, Pang Y, Wang J, et al. Explorative study of rotary tube piercing process for producing titanium alloy thick-walled tubes with bi-modal microstructure. Arch Civ Mech Eng 2018;18:1451–63. https://doi.org/10.1016/j.acme.2018.05.005.
[6] Nikitin MV, Maslyuk VM, Lazko NV. Improving the wear resistance of structural steels through the use of metallurgical production factors. Metallurgist 2010;54:28–32. https://doi.org/10.1007/s11015-010-9249-6.
[7] Skripalenko MM, Bazhenov VE, Romantsev BA, Skripalenko MN, Huy TB, Gladkov YA. Mannesmann piercing of ingots by plugs of different shapes. Mater Sci Technol 2016;32:1712–20. https://doi.org/10.1080/02670836.2016.1145840.
[8] Fourment L, Chenot JL, Mocellin K. Numerical formulations and algorithms for solving contact problems in metal forming simulation. Int J Numer Methods Eng 1999;46:1435–62. https://doi.org/10.1002/(SICI)1097-0207(19991130)46:9<1435::AID-NME707>3.0.CO;2-9.
[9] Chastel Y, Diop A, Fanini S, Bouchard PO, Mocellin K. Finite element modeling of tube piercing and creation of a crack. Int J Material Form 2008;1:355–8. https://doi.org/10.1007/s12289-008-0068-2.
[10] Fernandes M, Marouf N, Montmitonnet P, Mocellin K. Impact of the different friction coefficients on the tools on the mechanics of the Mannesmann 2-roll tube piercing. ISIJ Int 2020;60:2917–26. https://doi.org/10.2355/isijinternational.ISIJINT-2020-290.
[11] Ceretti E, Giardini C, Brisotto F. 2D simulation and validation of rotary tube piercing process. AIP Conf Proc 2004;712:1154–9. https://doi.org/10.1063/1.1766684.
[12] Topa A, Kim DK, Kim Y. 3D numerical simulation of seamless pipe piercing process by fluid-structure interaction method. MATEC Web Conf 2018;203.
[13] Murillo-Marrodán A, García E, Cortés F. A study of friction model performance in a skew rolling process numerical simulation. Int J Simulat Model 2018;17(4):569–82. https://doi.org/10.2507/IJSIMM17(4)441.
[14] Derazkola HA, García Gil E, Murillo-Marrodán A, Méresse D. Review on dynamic recrystallization of martensitic stainless steels during hot deformation: Part I—experimental study. Met 2021:11.
[15] Murillo-Marrodán A, García E, Cortés F. Modelling of the cone-type rotary piercing process and analysis of the seamless tube longitudinal shear strain using industrial data. AIP Conf Proc 2019;2113:40003. https://doi.org/10.1063/1.5112537.

[16] No Title Available online: https://www.tubosreunidos.com/.
[17] Ghiotti A, Fanini S, Bruschi S, Bariani PF. Modelling of the Mannesmann effect. CIRP Ann 2009;58:255–8. https://doi.org/10.1016/j.cirp.2009.03.099.
[18] Romantsev BA, Skripalenko MM, Huy TB, Skripalenko MN, Gladkov YA, Gartvig AA. Computer simulation of piercing in a four-high screw rolling mill. Metallurgist 2018;61:729–35. https://doi.org/10.1007/s11015-018-0556-7.
[19] Komori K. Simulation of Mannesmann piercing process by the three-dimensional rigid-plastic finite-element method. Int J Mech Sci 2005;47:1838–53. https://doi.org/10.1016/j.ijmecsci.2005.07.009.